Detecting China's Urban Expansion Over the Past Three Decades Using Nighttime Light Data

Pengfeng Xiao, *Member*, *IEEE*, Xiaohui Wang, Xuezhi Feng, Xueliang Zhang, and Yongke Yang

***Abstract*—China has experienced a rapid urban expansion over the past three decades because of its accelerated economic growth. In this study, we detected and analyzed the urban expansion of China during this period using multi-temporal Defense Meteorological Satellite Program Operational Linescan System (DMSP-OLS) nighttime light data and multi-source Normalized Difference Vegetation Index (NDVI) data. First, an intercalibration was performed to improve the continuity and comparability of the nighttime light data from 1992 to 2010. The nighttime light and NDVI data were then subjected to a local support vector machine (SVM) based region-growing method to extract the urban areas from 1992 to 2010. The urban areas from 1981 to 1991 were identified using the areas in 1992 and NDVI data, based on the hypothesis that China's urban expansion continued during this period. Finally, the extracted time-series urban maps were validated with Landsat images. The proposed local SVM-based region-growing method performed better than a local thresholding method and a global SVM-based region-growing method according to visual and quantitative comparisons of the urban boundaries and areas. We also analyzed the expansion rates to understand the dynamics of the urban areas in China and in its seven economic regions. In particular, the urban expansion patterns were investigated in three typical urban agglomerations, i.e., Beijing–Tianjin–Hebei, Yangtze River Delta, and Pearl River Delta. The proposed urban expansion direction, urban expansion intensity, and relative ratio of urban expansion demonstrated the regional variation among the three urban agglomerations.**

***Index Terms*—Change detection algorithms, land surface, remote sensing, support vector machines (SVMs), urban areas.**

I. Introduction

URBANIZATION has been a significant feature of the development of China's society since the country adopted an economic reform and openness policy in 1978. Urban areas concentrate people, infrastructure, and economic activities. Thus, urbanization is simultaneously a demographic, economic, and land-use change phenomenon [1], which means that it is very important to map the urban expansion of China over the past three decades. Historically, optical remote sensing data have been used to map China's urban areas and the expansion of urban land-cover for individual cities, e.g., Shanghai [2], Guangzhou [3], [4], Nanjing [5], and Shijiazhuang [6], or local regions, e.g., Beijing–Tianjin–Hebei [7], Bohai Rim [8], Yangtze River Delta [9], and Pearl River Delta [10]–[12], whereas little research has focused on the national scale patterns of urban expansion [13]–[18].

China's urban extent is difficult to detect at a national scale using coarse-resolution remote sensing because of the tiny size of the urban area relative to the total land area. Fine-resolution remote sensing of urban area is also challenging because of the spectral and spatial complexity of the land cover within cities. Fortunately, in contrast to most traditional sensors, nighttime light sensors have the unique capacity to map human activities from space [19], [20]. The most commonly used nighttime light sensor is the Operational Linescan System (OLS) onboard the U.S. Defense Meteorological Satellite Program (DMSP), which has been in operation since the early 1970s. The sensor has a unique low-light imaging capability, which was developed for detecting clouds based on moonlight. In addition to moonlit clouds, the OLS also detects lights from human settlements, fires, gas flares, heavily lit fishing boats, lightning, and the aurora [21], [22]. The potential use of OLS data for the observation of city lights and other visible and near-infrared emission sources was first noted in the 1970s. Many previous studies have employed OLS images to demonstrate their application in different areas, e.g., as indicators of urban dynamics [1], [23]–[26], population levels [27]–[31], economic activities [32], gas emissions [33], and armed conflicts [34].

Nighttime light images have some advantages over daytime images because they measure emitted rather than reflected radiation, which avoids certain classification problems when separating developed versus nondeveloped land cover [29]. However, DMSP-OLS data still have several limitations related to their coarse spatial resolution, saturation in bright urban cores, and single spectral band, as well as inconsistencies in their radiometric properties within and between scenes and sensors. Moreover, the biggest problem when using the nighttime light data as a proxy measure of the urban extent is that the lighted areas detected by OLS are consistently larger than the geographic extents of the settlements with which they are associated. The larger spatial extent of the lighted area relative to the urban area is sometimes referred to as blooming [35]. To offset the blooming effect, Imhoff *et al.* proposed the use of a threshold with an 89%

Manuscript received October 12, 2013; revised January 19, 2014; accepted January 24, 2014. Date of publication February 27, 2014; date of current version December 22, 2014. This work was supported in part by the National Key Basic Research Program on Global Change (Grant 2011CB952001), and in part by a project funded by the Priority Academic Program Development (PAPD) of Jiangsu Higher Education Institutions.

The authors are with the Jiangsu Provincial Key Laboratory of Geographic Information Science and Technology, Nanjing University, Nanjing 210023, China, the Key Laboratory for Satellite Mapping Technology and Applications of State Administration of Surveying, Mapping and Geoinformation of China, Nanjing University, Nanjing 210023, China, and the Department of Geographic Information Science, Nanjing University, Nanjing 210023, China (e-mail: xiaopf@nju.edu.cn).

Color versions of one or more of the figures in this paper are available online at http://ieeexplore.ieee.org.

Digital Object Identifier 10.1109/JSTARS.2014.2302855

detection frequency to eliminate less frequently detected lighted pixels at the peripheries of large urban areas [36]. A subsequent analysis obtained a correlation of 0.68 between Ln(lighted area) and Ln(population) when using a threshold of 80% [29]. However, the authors also highlighted the limitations of using a single threshold during a global analysis.

Several methods are available for extracting urban information from nighttime light data, including an empirical thresholding technique [37], [38], a thresholding technique based on mutation detection [39], a statistical data comparison method [8], [40], a high-resolution data comparison method [41], [25], and an image-classification method [24], [26], [42]. Henderson *et al.* developed a thresholding technique that used ancillary data, where they examined three urban areas as they appeared in both OLS images and Landsat images on approximately the same dates [41]. Then light thresholds were calculated for each city by minimizing the discrepancies between the OLS- and Landsat-derived urban boundaries. To address the problems of thresholding methods using empirical strategies or manual trial- and-error procedures, Cao *et al.* proposed a support vector machine (SVM) based region-growing algorithm for the semi-automatic extraction of urban areas from OLS data [24]. Several simple criteria were used to select the SVM training sets of urban and nonurban pixels, where an iterative classification and training procedure were used to identify the urban pixels. However, it was difficult to accurately extract urban areas in China using a single classifier because of the high regional variation in the physical geography and economic development status [25], [35]. Thus, Liu *et al.* developed a threshold method followed a procedure of dividing the research area into several economic regions [25].

Previously, the dynamics of urban expansion in China from 1992 to 2008 were extracted using OLS data [25]. To illustrate the urban expansion in China over the past three decades, which has occurred as a consequence of economic reform and openness policy, we developed a new method for extracting China's urban expansion during 1981–2010 using multi-temporal OLS data and multi-source Normalized Difference Vegetation Index (NDVI) data. First, an intercalibration was implemented to improve the continuity and comparability of nighttime light data from 1992 to 2010. The nighttime light and NDVI data were then subjected to a local SVM-based region-growing method to extract the urban areas from 1992 to 2010. Next, the urban areas from 1981 to 1991 were extracted using the areas in 1992 and NDVI data, based on the hypothesis that China's urban areas are expanded continuously during this period. Finally, the extracted time-series urban maps were validated with Landsat images, and spatial changes were analyzed to understand the dynamics of the urban areas in China and in its seven economic regions, as well as three urban agglomerations over the past three decades.

II. Data

A. DMSP-OLS Data

The DMSP-OLS derived version 4 nighttime light dataset is a freely available product obtained from the U.S. National Geophysical Data Center (NGDC) (http://ngdc.noaa.gov/eog/dmsp/downloadV4composites.html). This dataset includes images acquired by six different DMSP satellites, i.e., F10, F12, F14, F15, F16, and F18. In cases where two satellites were collecting data, two separate composites were produced [33]. The files are cloud-free composites, which were made using all the available archived OLS smooth resolution data from 1992 to 2010. The products are 30 arc-second grids, which span -180° to 180° longitude and -65° to 75° latitude. The radiometric resolution of the dataset is 6 bits, i.e., the digital number (DN) ranges from 0 to 63.

The average DN values and the number of lit pixels differed between two satellites in the same year [25], [26]. Thus, based on the data selection method proposed by Liu *et al.* [25], we selected the one with better continuity and comparability from the two sets of data, i.e., the selected image dataset included the data products from F10 (1992, 1993, and 1994), F12 (1995 and 1996), F14 (1997, 1998, 1999, 2000, 2001, and 2002), F15 (2003, 2004, 2005, and 2006), F16 (2007, 2008, and 2009), and F18 (2010). After obtaining the time-series global nighttime light data from 1992 to 2010, China's nighttime light data were extracted according to the national boundaries. Next, they were reprojected onto the Lambert Conformal Conic Projection and resampled to a pixel size of 1 km to facilitate the calculations.

B. NDVI Data

Two types of NDVI data were used, i.e., Système Probatoire Pour l'Observation de la Terre (SPOT) Vegetation (VGT) derived NDVI and Advanced Very High Resolution Radiometer (AVHRR) derived NDVI. The former had 1-km resolution and was used for urban area extraction and correction from 1998 to 2010, whereas the latter had 5-km resolution and was used for urban area extraction and correction from 1981 to 1997 because NDVI data were not available with 1-km resolution before 1998.

The SPOT-VGT NDVI data were obtained from SPOT-VGT (http://free.vgt.vito.be), which is a program founded by France in cooperation with Belgium, Italy, and Sweden, where the archive became operational in 1998. The present study used the 10-day maximum value composites of SPOT-VGT NDVI during July from 1998 to 2010 at 1-km resolution.

The AVHRR NDVI data were obtained from the Land Long Term Data Record (LTDR) (http://ltdr.nascom.nasa.gov), which is a project funded by U.S. National Aeronautics and Space Administration (NASA). The 10-day maximum value composites of AVHRR NDVI during July from 1981 to 1997 at 5-km resolution were resampled to 1-km resolution.

C. Landsat Data

We used Landsat images acquired from 1981 to 2010 to validate the urban areas extracted based on the OLS and NDVI data. The Multispectral Scanning System (MSS) images had a spatial resolution of 60 m, and the Thematic Mapper (TM) images and Enhanced Thematic Mapper Plus (ETM+) images had a spatial resolution of 30 m. The Landsat data were obtained from the Earth Science Data Interface (ESDI) at the Global Land Cover Facility (GLCF) from the University of Maryland (UMD) (http://glcfapp.glcf.umd.edu:8080/esdi/index.jsp) and the United States Geological Survey (USGS) Global Visualization Viewer (GloVis) (http://glovis.usgs.gov/index.shtml).

TABLE I
COEFFICIENTS OF THE SECOND-ORDER REGRESSION MODELS FOR DMSP-OLS DATA INTERCALIBRATION

Satellite	Year	*a*	*b*	*c*	R^2
F10	1992	0.002	0.903	–0.021	0.812
	1993	0.003	1.027	–0.194	0.800
	1994	0.004	0.941	–0.093	0.828
F12	1995	0.008	0.509	2.529	0.714
	1996	0.008	0.581	1.916	0.736
F14	1997	0.002	0.993	1.043	0.756
	1998	0.004	0.874	0.559	0.792
	1999	0.001	1.105	0.882	0.786
	2000	0.004	0.758	1.190	0.879
	2001	–0.001	1.034	–0.607	0.713
	2002	–0.005	1.328	0.794	0.918
F15	2003	–0.011	1.712	–0.925	0.867
	2004	–0.008	1.531	–0.184	0.916
	2005	–0.003	1.314	0.128	0.919
	2006	–0.004	1.248	1.056	0.901
F16	2007	0	1	0	1
	2008	0.003	0.755	1.634	0.893
	2009	0.007	0.436	2.354	0.903
F18	2010	0.009	0.188	3.580	0.817

III. METHOD

A. Intercalibration of DMSP-OLS Data

The OLS lacks on-board calibration, so the individual composites were intercalibrated via an empirical procedure using a second-order polynomial regression equation to improve the continuity and comparability of the nighttime light data from 1992 to 2010. The intercalibration method for global nighttime light data was developed by Elvidge *et al.* [33]. Subsequently, Liu *et al.* proposed an intercalibration approach for China based on this method and the actual urban development situation in China [25], which was used in the present study.

The city of Jixi in Heilongjiang Province was selected as the reference area of calibration because of its relatively stable economic development and the high conformity of DN values over different years. The nighttime light data from satellite F16 in 2007 were selected as the reference data because they had the highest cumulative DN value. A series of second-order regression models was implemented for each satellite using (1) and empirical coefficients, which were derived by comparing the DN values from other images with the reference data from satellite F16 in 2007 for the city of Jixi. Table I shows the coefficients and the respective R^2 values obtained from the intercalibration. Finally, the intercalibrated data were rescaled to 6 bits.

$$DN' = a \times DN^2 + b \times DN + c \tag{1}$$

where DN is the original DN value, DN' is the intercalibrated DN value, and a, b, and c are the coefficients of the second-order regression model.

B. Extracting Urban Areas

The urban areas from 1992 to 2010 were directly extracted from OLS data using the local SVM-based region-growing method. It was difficult to extract urban information for China using a single classifier because of the high regional variation in the physical geography and economic development status [25], [35], so we divided China into seven economic regions, as shown in Table II, according to a partitioning strategy that integrated Clustered Economic Regions and Coordinated Economic Regions [43], which reflect regional variations in economic development and urbanization, i.e., Northeast Region, Northwest Region, North Region, East Region, Central Region, South Region, and Southwest Region. The local SVM-based region-growing method was implemented for each economic region.

TABLE II
SEVEN ECONOMIC REGIONS OF CHINA USED FOR URBAN EXTRACTION

Economic region	Provinces
Northeast Region	Liaoning, Jilin, Heilongjiang
Northwest Region	Shaanxi, Gansu, Qinghai, Ningxia, Xinjiang
North Region	Beijing, Tianjin, Hebei, Inner Mongolia, Shanxi
East Region	Shandong, Shanghai, Jiangsu, Zhejiang
Central Region	Henan, Anhui, Jiangxi, Hubei, Hunan
South Region	Fujian, Guangdong, Guangxi, Hainan, Taiwan, Hong Kong, Macao
Southwest Region	Sichuan, Guizhou, Yunnan, Tibet, Chongqing

A SVM is a nonparametric method based on statistical learning theory, which overcomes the problems associated with empirical strategies or manual trial-and-error procedures when applying thresholding methods to nighttime light data [44]. We used a previously developed SVM-based region-growing algorithm [24] to semi-automatically distinguish urban pixels from the nonurban background in each economic region. The basic concept employed by a SVM is to classify the input vectors into two classes using the hyperplane with the maximal margin, which is derived by solving the constrained quadratic programming problem shown in (2). The advantage of SVM-based classifiers is that they are better at solving learning problems when only a small number of training samples are available.

$$\text{Maximize } W(\alpha) = \sum_{i=1}^{n} \alpha_i - \frac{1}{2} \sum_{i=1}^{n} \sum_{j=1}^{n} \alpha_i \alpha_j y_i y_j K(x_i, x_j)$$
$$\text{Subject to } \left\{ \sum_{i=1}^{n} \alpha_i y_i = 0 \text{ and } 0 \le \alpha_i \le T \text{ for } i = 1, 2, \ldots, n \right\} \tag{2}$$

where $x_i \in R_d$ are the training sample vectors, $y_i \in \{-1, +1\}$ are the corresponding class labels, and $K(u, v)$ is the kernel function. The radial basis function was selected as the kernel function and the free parameter γ (gamma) was set as 1 in the present study.

The SVM-based region-growing procedure was performed as follows. First, two training sets were automatically selected as urban and nonurban dataset from the OLS and NDVI data. In the urban training set, the pixels selected were the maximum in each four-neighborhood, where OLS DN >30, whereas the nonurban training set included water pixels with NDVI values <0, vegetation pixels with NDVI values >0.4, and pixels with OLS values <30. These thresholds only served as a baseline for selecting the training samples for urban and nonurban pixels. After SVM training using these two datasets, the SVM-based classifier was applied to the OLS and NDVI data to classify the unknown pixels.

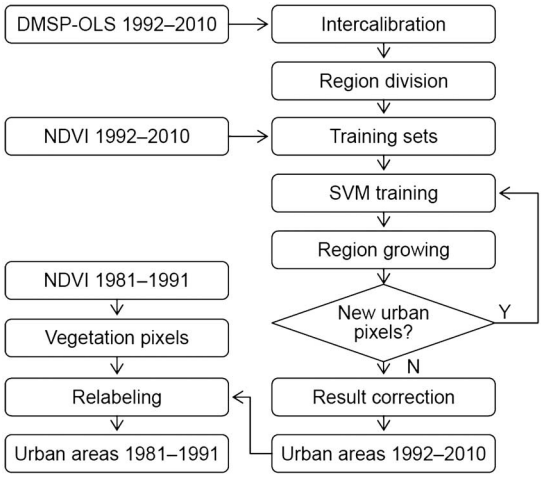

Fig. 1. Flowchart of producing time-series of urban areas for China from 1981 to 2010 based on DMSP-OLS nighttime light data and NDVI data.

However, we did not classify all of the unknown pixels at the same time. Instead, we integrated the SVM classifier into an iterative region-growing procedure, which classified the pixels near the urban training pixels in a step-by-step manner. During the first step, the pixels in the urban training sets were assigned as seeds, then all of the pixels within a 3×3 window for each seed were classified simultaneously using the SVM-based classifier. After the classification was completed, the pixels that were newly classified as urban in this step were added to the training set and the SVM classifier was retrained based on the new training set. In each successive step, the newly classified urban pixels from the former step were used as seed pixels. This iterative procedure was implemented many times until there is no new urban pixels were identified. After the SVM-based region-growing procedure, the urban area map was refined further by removing pseudo-urban pixels with NDVI values >0.55.

According to the previous research, the SVM-based region-growing method works better for developed regions than underdeveloped regions [24]. This is because regional variation results in differences in the urban training set and the region-growing procedure. Thus, we divided China into seven economic regions and implemented the SVM-based region-growing procedure separately for each economic region, which we refer to as the local SVM-based region-growing method. The flowchart of producing time-series of urban areas for China is shown in Fig. 1.

We also compared the performance of the new method with that of the Landsat-assisted local thresholding method [41] and the global SVM-based region-growing method [24]. The local thresholding method set the optimal DN threshold for each economic region by matching the urban areas of the training cities derived from the OLS data to the Landsat-delineated urban areas as closely as possible. The global SVM-based region-growing method implemented the region-growing procedure for all of the pixels.

C. Mapping Urban Areas from 1992 to 2010

Using the local SVM-based region-growing method, urban areas were extracted from the OLS and NDVI data, and the dynamics of urban expansion in China from 1992 to 2010 were mapped. We selected eight results with intervals of 2 or 3 years, i.e., 1992, 1995, 1998, 2000, 2003, 2005, 2008, and 2010, to produce time-series for the urban areas.

Due to intercalibration and classification errors, some pixels were classified as urban in the early years but as nonurban in the later years. A conditional statement was used to re-label these pixels as urban in the later years based on an assumption that the urban areas in China did not decrease over the past three decades [26], [40]. After this correction, the final time-series of urban areas was obtained for the period 1992–2010.

D. Mapping Urban Areas from 1981 to 1991

The 1980s was the first decade after China adopted the economic reform and openness policy. Unfortunately, no nighttime light data were available for extracting urban areas during this period. Thus, we used the NDVI data in July from 1981 to 1991 and the urban areas in 1992 to extract the urban areas during this period. Based on assumptions that urban areas did not decrease during this period and that they were mostly converted from vegetation areas, especially cropland [15], [18], the urban extent during this period must have been within that in 1992. Thus, the vegetation pixels within the urban extent in 1992 were removed and the remained pixels were considered to be urban pixels during this period. The manual thresholding strategy was used to identify the vegetation pixels, where an NDVI threshold of 0.55 was adopted, i.e., the urban pixels in 1992 with NDVI values >0.55 in each year between 1981 and 1991 were labeled as nonurban pixels in this year. The outputs from 2 years, i.e., 1981 and 1985, were selected to produce time-series of urban areas for the period 1981–1991. Finally, we obtained the urban areas of China during 10 phases over the past 30 years.

E. Measuring Urban Expansion

To measure the urban expansion of China using the time-series of the urban areas, we used the urban expansion rate to indicate the national and regional urban growth, the urban expansion intensity, the relative ratio of urban expansion, and the urban expansion direction to indicate the regional variation in urban expansion.

1) Urban Expansion Rate: The urban expansion rate represents the average annual urban area growth in a period, which measures the speed of urban expansion.

$$UER = (A_2 - A_1)/(T_2 - T_1) \tag{3}$$

where UER is the urban expansion rate ($\mathrm{km}^2/\mathrm{year}$), and A_1, A_2 are the urban areas (km^2) in the years T_1, T_2, respectively.

2) Urban Expansion Intensity: The urban expansion intensity represents the urban expansion rate per unit land area, which is used to compare the strength of urban expansion among regions.

$$UEI = 100 \cdot UER/A_R \tag{4}$$

where UEI is the urban expansion intensity (/year), UER is the urban expansion rate ($\mathrm{km}^2/\mathrm{year}$), and A_R is the total area of the region (km^2).

3) Relative Ratio of Urban Expansion: The relative ratio of urban expansion represents the ratio of the urban expansion rate of a certain region relative to that of the overall area, which is used to compare the urban expansion rate among regions.

$$RRUE = \frac{(S_2 - S_1) \cdot A_1}{S_1 \cdot (A_2 - A_1)} \tag{5}$$

where $RRUE$ is the relative ratio of urban expansion for a certain region, S_1, S_2 are the urban areas in the region (km^2), and A_1, A_2 are the urban areas in the whole of China (km^2) in the years T_1, T_2, respectively.

4) Urban Expansion Direction: The urban expansion direction is illustrated by the shift of the urban centroid. The centroid of a city is the arithmetic mean position of all the points in the urban area. After defining a geographical coordinate system, the centroid of a nonself-intersecting closed polygon defined by n vertices $(x_0, y_0), (x_1, y_1), \ldots, (x_{n-1}, y_{n-1})$ is the point (C_x, C_y), where

$$C_x = \frac{1}{6A}\sum_{i=0}^{n-1}(x_i + x_{i+1})(x_i y_{i+1} - x_{i+1} y_i) \tag{6}$$

$$C_y = \frac{1}{6A}\sum_{i=0}^{n-1}(y_i + y_{i+1})(x_i y_{i+1} - x_{i+1} y_i) \tag{7}$$

and where A is the polygon's signed area (km^2).

$$A = \frac{1}{2}\sum_{i=0}^{n-1}(x_i y_{i+1} - x_{i+1} y_i). \tag{8}$$

Given the expansion direction of a cluster of urban, the centroid (C'_x, C'_y) is computed by integrating the centroid of the urban patches using the area of each patch as a weight:

$$C'_x = \sum_{i=1}^{m}(A_i C_{xi}) / \sum_{i=1}^{m} A_i \tag{9}$$

$$C'_y = \sum_{i=1}^{m}(A_i C_{yi}) / \sum_{i=1}^{m} A_i \tag{10}$$

where m is the number of urban patches in the region, and A_i and (C_{xi}, C_{yi}) are the area (km^2) and the centroid of the ith urban patch, respectively.

IV. Results

A. Urban Extraction Accuracy Assessment

1) Comparing With Landsat Images: Landsat images were used to evaluate the urban extraction results because the spatial resolutions of the Landsat MSS (60 m) and TM/ETM+ (30 m) images were much finer than that of the OLS data (1 km) [25], [34], [35], [40], [41]. The urban land was delineated manually in Landsat images as the reference data and the accuracy assessment, which involved both the urban boundaries and areas, was performed using the OLS-derived urban areas. The results obtained with the three methods were compared, i.e., the local thresholding method [41], the global SVM-based region-growing method [24], and the proposed local SVM-based region-growing method.

Fig. 2 shows the urban boundaries of seven selected cities in 2000, i.e., Tianjin, Zhengzhou, Wuhan, Nanjing, Xiamen, Lhasa, and Jilin. The seven cities were selected from seven economic regions with different levels of urban development. The lighted areas of each city in the OLS images were highly consistent with the Landsat-delineated urban boundaries, which validates the potential use of OLS data for the extraction of urban areas. The local thresholding method tended to identify simple and compact urban areas because of the blooming of the OLS data, whereas the SVM-based methods extracted detailed urban areas with the region-growing procedure and they rejected vegetated and water pixels based on the SVM classifier and NDVI criteria. The results obtained with the proposed local SVM-based region-growing method retained more details than those with the global SVM-based region-growing method (e.g., Zhengzhou, Wuhan, and Lhasa), which was a result of implementing the region-growing procedure for each economic region.

Fig. 3 shows the total accuracy for 22 cities in 2000, which was assessed by comparing the urban areas derived from OLS images with those delineated from Landsat images. The total accuracy was calculated based on the error matrix from the two results for each city. Cities with different levels of urban development were selected from seven economic regions, i.e., Shenyang, Haerbin, Jilin, and Suihua in Northeast Region; Xi'an and Xining in Northwest Region; Beijing, Tianjin, and Baotou in North Region; Nanjing, Hangzhou, and Dongying in East Region; Wuhan, Zhengzhou, and Hefei in Central Region; Xiamen, Fuzhou, and Liuzhou in South Region; Chengdu, Guiyang, Lhasa, and Dali in Southwest Region. Two, one, and three cities had area accuracies $>95\%$; 14, 16, and 16 cities were within the range 60%–95%; and six, five, and three cities were within the range $<60\%$ using the local thresholding method, global SVM-based region-growing method, and proposed local SVM-based region-growing method, respectively. The three methods delivered similar performance in the high-accuracy range, but the proposed method had fewer cities in the low-accuracy range compared with the other two methods.

2) Comparing With Google Earth Images: We also use 120 validation samples from Google Earth to evaluate the accuracy of the proposed method in 2000, 2005, and 2010, as shown in Table III. The 120 urban samples with areas of 1×1 km were selected randomly from 120 different cities in China. A comparison of the samples and the proposed urban extraction results showed that the consistency ratios were 74.52%, 84.70%, and 88.44% in 2000, 2005, and 2010, respectively.

3) Comparing With High-Resolution Land Use Products: We also compared the proposed method with the more accurate results produced by Liu *et al.* [46], who released the land use products of China for 1990, 1995, and 2000 in 1-km resolution, which were produced based on 30-m resolution Landsat TM images via human interpretation. The released products recorded area fractions of different land use types within each pixel. Thus, we accumulated the pixels where the urban fraction comprised $>70\%$ to determine China's total urban area. A comparison of

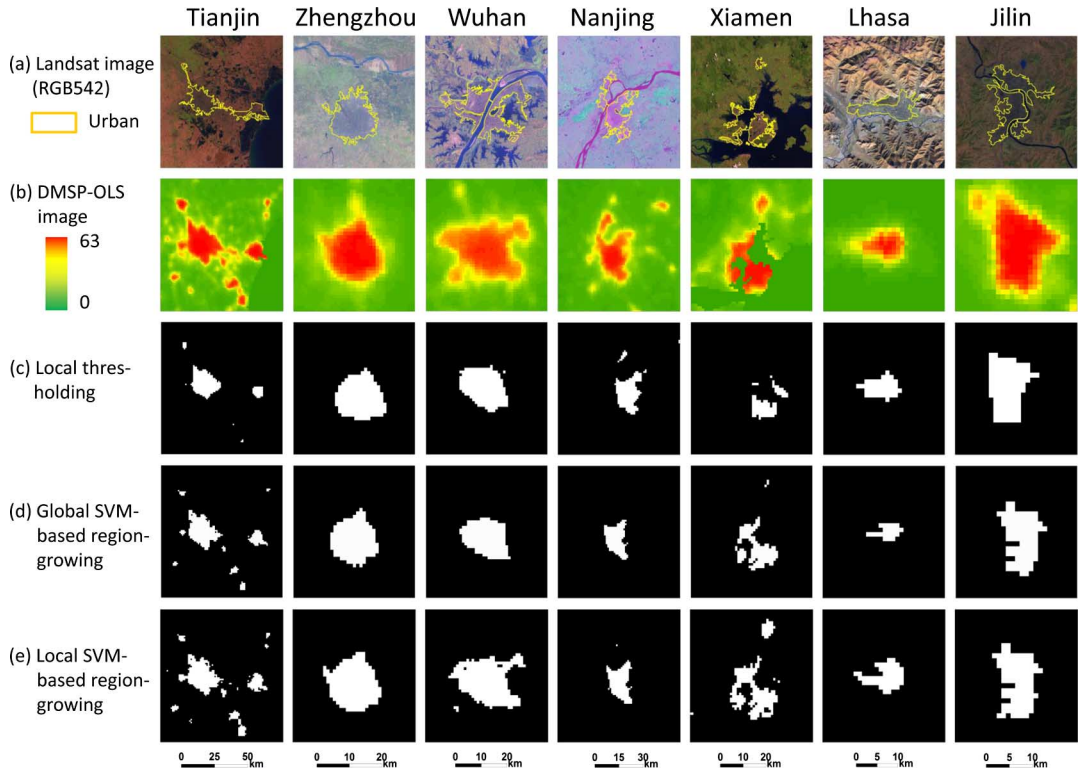

Fig. 2. Boundary comparison for seven urban areas extracted from OLS data in 2000. Note that the local thresholding method produces simple and compact boundaries, and the proposed local SVM-based region-growing method produces more details than the global method.

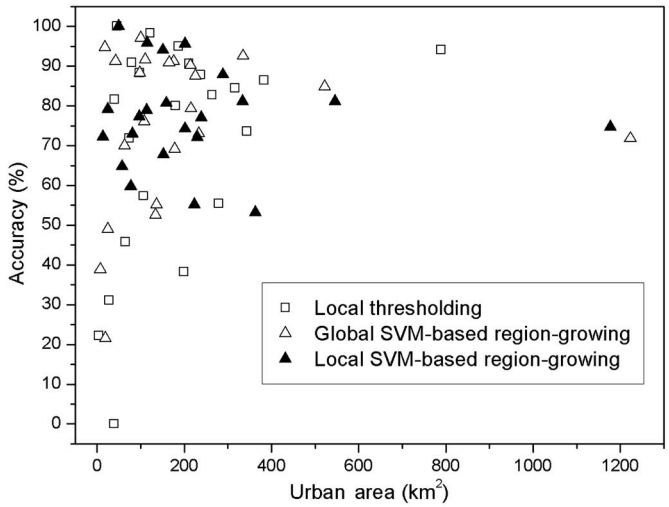

Fig. 3. Accuracy for 22 urban areas in 2000 using three methods. Note that the proposed local SVM-based region-growing method had fewer cities in the low-accuracy range than the other two methods.

TABLE III
URBAN EXTRACTION ACCURACY CALCULATED BASED ON 120 VALIDATION SAMPLES FROM GOOGLE EARTH

Year	2000	2005	2010
Accuracy (%)	74.52	84.70	88.44

TABLE IV
COMPARISON OF CHINA'S TOTAL URBAN AREA ACCORDING TO LIU *ET AL.* AND THE RESULTS OBTAINED WITH THE PROPOSED METHOD

Year	1990	1995	2000
Liu *et al.* (km^2)	12 067	16 727	17 967
Proposed method (km^2)	9 263	11 241	19 073
Consistency ratio (%)	76.76	67.20	93.84

the urban areas reported by Liu *et al.* and the results obtained with our proposed method showed that the consistency ratios were 76.76%, 67.20%, and 93.84% in 1990, 1995, and 2000, respectively, as shown in Table IV.

B. Total Urban Expansion in China

After obtaining the urban area products, we produced time-series urban area maps for China. However, the urban area only occupied 0.70% of the total land area even in 2010, so the urban changes were difficult to distinguish visually in the maps. Thus, the urban area maps of the whole country are not presented in the paper. Instead, we present an analysis of the urban expansion rate in China and the maps for typical regions.

Fig. 4 shows that the urban areas in China have increased exponentially during the last 30 years as a consequence of accelerated urbanization, which agrees with the result of determining China's urban expansion from 1990 to 2010 using optical satellite remote sensing [18]. The total extracted urban area for China was 5 694 km^2 in 1981, with an average growth rate of 11.74% per year in the following 20 years. In 2000, the urban

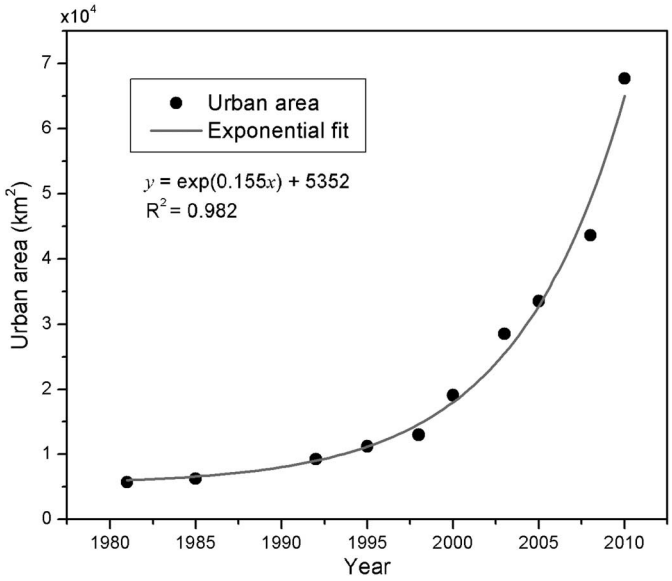

Fig. 4. China's urban area growth from 1981 to 2010. Note that the growth in the last 10 years was remarkably faster than that in the previous 20 years.

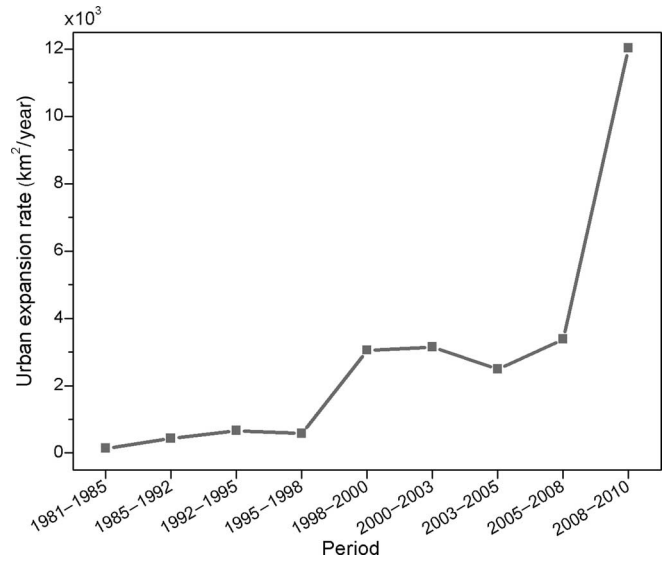

Fig. 5. China's urban expansion rate from 1981 to 2010. Note the low rate from 1981 to 1998, the high rate from 1998 to 2008, and the maximum rate from 2008 to 2010.

area was 19 073 km^2, while a sharp increase of 25.49% per year occurred in the following 10 years. In 2010, urban area reached 67 694 km^2, which was 11.89 times bigger than that in 1981. Thus, China's urban area experienced a dramatic expansion over the past 30 years.

The three stages of urban area growth can be observed more clearly based on the urban expansion rate shown in Fig. 5. From 1981 to 1998, the urban expansion area maintained a low-level increase of 428 km^2 per year. From 1998 to 2008, however, the rate accelerated rose to a high level of 3 067 km^2 per year. From 2008 to 2010, it reached a maximum rate of 12 028 km^2 per year. The urban areas will probably continue to increase in the next decades as a consequence of China's sustainable and stable economic development in recent years.

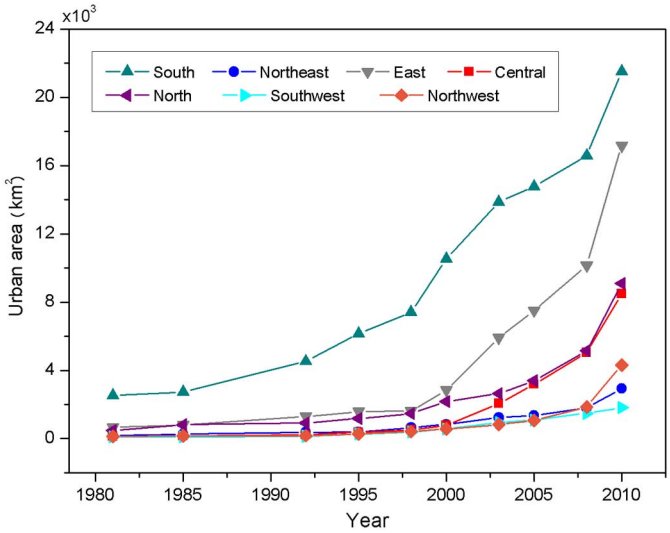

Fig. 6. Urban area growth in the seven economic regions during 1981–2010. Note that the South Region had the biggest urban area and the highest expansion rate. The East Region had the second highest area, followed by the North Region and Central Region.

C. Urban Expansion in Seven Economic Regions

The great regional variations in the economic development status in China led to remarkable differences in urban expansion during 1981–2010, as shown in Fig. 6. The South Region had the biggest urban area and expansion rate among the seven economic regions, which began to increase significantly as early as 1985. The East Region was the second, with a very high upward trend from 1998. Next were the North and Central Regions with gradual rises from 1998 and 2000, respectively. The Northwest, Northeast, and Southwest Regions had the smallest urban areas and lowest expansion rates, with no apparent upward trend until 2008. Furthermore, the variations in the urban expansion rates of each economic region were also very high, which are analyzed in Section IV-D.

D. Urban Expansion in Three Urban Agglomerations

The national urban expansion pattern is difficult to describe because of high regional variation and the small proportion of urban area relative to the total land area, whereas it can be observed more clearly in urban agglomerations. An urban agglomeration is an extended urban area, which comprises the built-up area of a central municipality and any suburbs linked via a continuous urban area. Three major rapidly developing urban agglomerations were selected from the 14 urban agglomerations in China, i.e., Beijing–Tianjin–Hebei, Yangtze River Delta, and Pearl River Delta [45], which are located in the rapidly developed North, East, and South Region, respectively, and we analyzed their urban expansions as follows.

1) Urban Expansion Pattern: The Beijing–Tianjin–Hebei urban agglomeration is located in the north of China, where it is bounded to the east by the Bohai Gulf portion of the Yellow Sea. It comprises 10 cities, including two municipalities, Beijing and Tianjin, and the surrounding cities of Shijiazhuang, Tangshan, Qinhuangdao, Baoding, Zhangjiakou, Chengde, Cangzhou, and Langfang, as shown in Fig. 7. It is one of the most important economic zones in China and it has experienced a

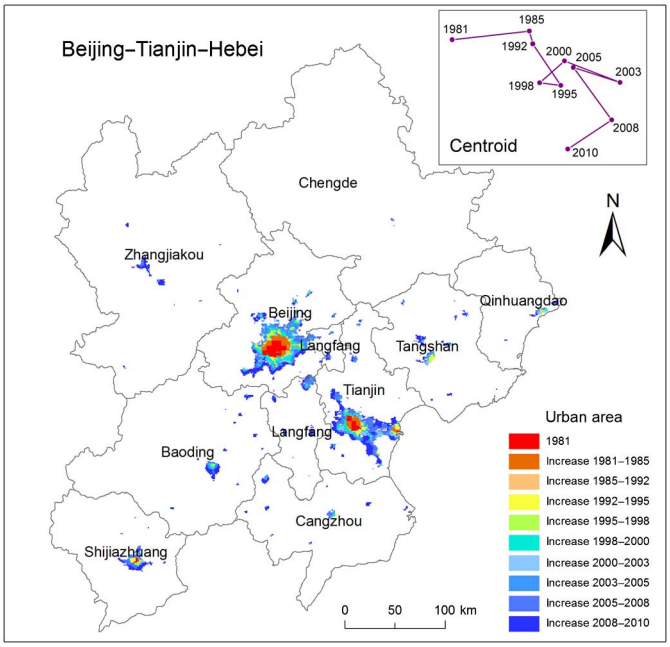

Fig. 7. Urban expansion and the shift of the centroid (top right) of the Beijing–Tianjing–Hebei urban agglomeration. The administrative boundaries of the cities are indicated by solid curves. Note the point-agglomeration pattern with the municipalities of Beijing and Tianjin, and the shift of the centroid from northwest toward southeast.

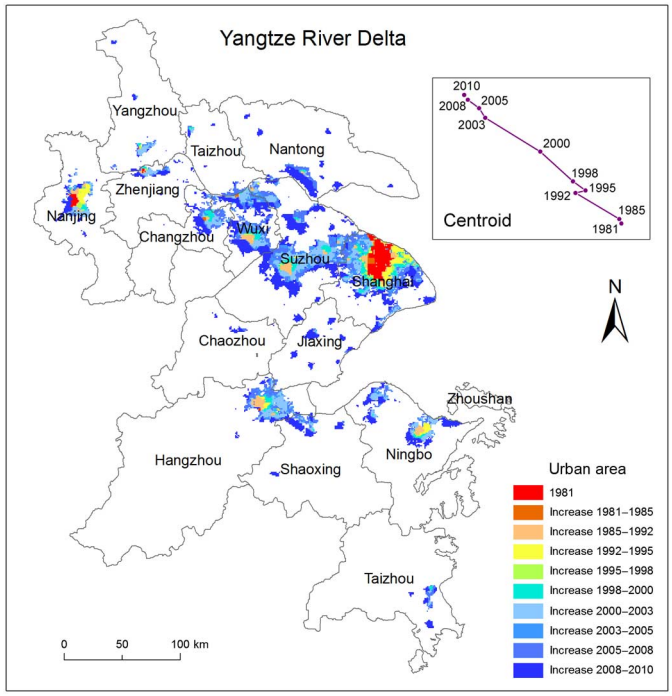

Fig. 8. Urban expansion and the shift of the centroid (top right) of the Yangtze River Delta urban agglomeration. The administrative boundaries of the cities are indicated by solid curves. Note the belt-agglomeration pattern with the central municipality of Shanghai and the shift of the centroid from southeast toward northwest.

rapid expansion over the past 30 years. However, the regional economic and social development is still imbalanced in the region. Differences in the structure of industry and technology, the effectiveness of energy utilization, and the goals of urban planning have resulted in a double-central urban expansion pattern. The distribution of the cities is dispersed, but Beijing and Tianjin have formed a point-agglomeration pattern during the period. The expansion trends indicate that Beijing has extended to the southwest (Fangshan District), northwest (Changping District), northeast (Huairou District), and east (Shunyi District), while Tianjin has tended to expand to the east (Binhai New Area), southeast (Jinnan District), and northwest (Wuqing District).

The Yangtze River Delta urban agglomeration is located in the east of China, where it is bounded to the east by the East China Sea. It comprises 16 cities, including the central municipality of Shanghai, eight cities in Jiangsu Province, i.e., Suzhou, Wuxi, Changzhou, Nanjing, Zhenjiang, Yangzhou, Taizhou, and Nantong, and six cities in Zhejiang Province, i.e., Hangzhou, Jiaxing, Huzhou, Ningbo, Shaoxing, Taizhou, and Zhoushan, as shown in Fig. 8. Since the 1980s, this urban agglomeration has experienced a major expansion, which was concentrated on Shanghai, Nanjing, Hangzhou, Suzhou, Wuxi, and Ningbo. This region has the most developed economy in China. In 2007, it only covered 1.5% of the total national land area, but 5.9% of the national population lived in the region and it generated nearly 20% of the gross domestic product (GDP) [32]. This region has a belt-agglomeration pattern with cores in Shanghai, Suzhou, Wuxi, and Changzhou. The region has already grown into the urban agglomeration that boasts the greatest economic strength, the largest industrial scale, and it is the most competitive force in China.

The Pearl River Delta urban agglomeration is located in the south of China, where it is bounded to the south by the South China Sea. It comprises nine cities in Guangdong Province, including the central municipality of Guangzhou, and the surrounding cities of Shenzhen, Zhuhai, Foshan, Jiangmen, Dongguan, Zhongshan, Zhaoqing, and Huizhou, as shown in Fig. 9. Guangdong Province was first selected for the economic reform experiment in 1978, where Shenzhen was China's first, and one of the most successful, Special Economic Zones. Special policies were proposed for the implementation and facilitation of economic reforms, which allowed various market processes to replace the planned economy. This region has experienced a very rapid urban expansion in the past 30 years, with the formation of a ring-agglomeration pattern along the Pearl River Estuary with the core of Guangzhou since early in the 1990s. This is the fastest growing region in China in terms of its industrial output, tertiary output, and export trade [10].

2) Urban Expansion Direction: The expansion direction of an urban agglomeration indicates the movement of the heart of the regional economy, which is affected by policy guidance, the population density, distance to road networks, distance to existing urban area, and other factors. In Figs. 7–9, the maps show the shift of the centroids over the past 30 years, thereby demonstrating the different expansion directions of the three urban agglomerations, which have been dominated by the regional geographic conditions and national policy guidance.

Although it has changed circuitously and repeatedly, the centroid of the Beijing–Tianjing–Hebei urban agglomeration has tended to shift from the northwest towards the southeast. From 1981 to 1995, it moved from the northwest toward the

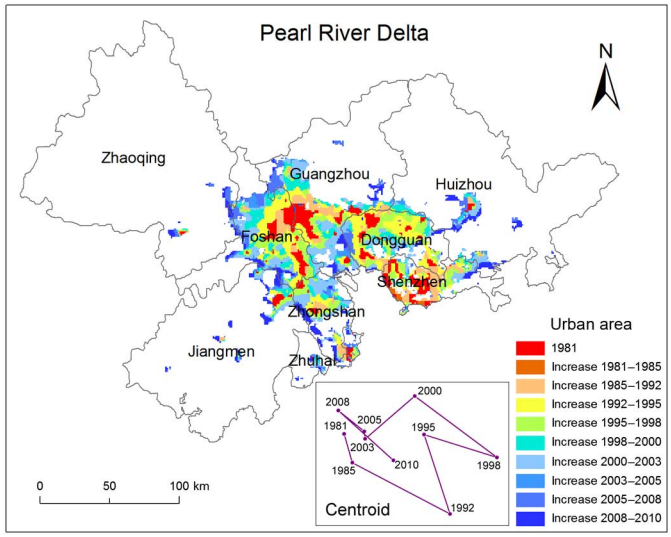

Fig. 9. Urban expansion and the shift of the centroid (bottom) of the Pearl River Delta urban agglomeration. The administrative boundaries of the cities are indicated by solid curves. Note the ring-agglomeration pattern with the central municipality of Guangzhou and the counterclockwise shift of the centroid.

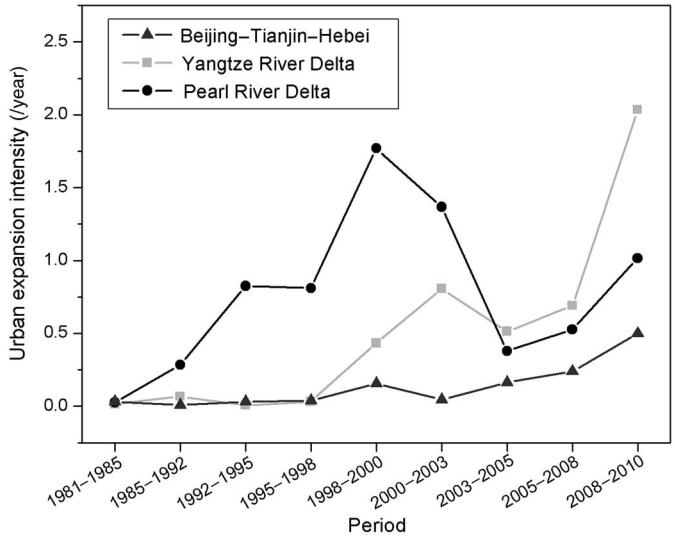

Fig. 10. Urban expansion intensities of the three urban agglomerations. Note the intense fluctuation in the value for the Pearl River Delta, the highest value for the Yangtze River Delta over the last decade, and the lowest value for the Beijing–Tianjin–Hebei.

southeast, but from 1995 to 1998, it experienced a short inverse change. From 1998 to 2003, it changed from west towards east, but from 2003 to 2005, it again made an inverse change. From 2005 to 2010, it began to shift from north to south again. The rapid expansion of Tianjin, especially the development of the Binhai New Area bounded by the Bohai Gulf since 1994, has contributed to the shift of the centroid.

In contrast, the centroid of the Yangtze River Delta urban agglomeration has moved dramatically from the southeast toward the northwest. With the exception of the short inverse change in 1995, the centroid shift pattern and trend has been steady, which is expected to continue in the future. Although Shanghai is the economic growth engine of the region, especially the Pudong New Area has expanded rapidly since 1992, the south area of Jiangsu Province, i.e., Suzhou, Wuxi, and Changzhou, has a higher population and more land for expansion than Shanghai, which has led to a shift of the centroid.

However, the centroid of the Pearl River Delta urban agglomeration has shifted counterclockwise during this period. From 1981 to 2003, it moved in a counterclockwise direction, with the exception of the change in 1995. From 2003 to 2008, it shifted from the southeast to the northwest, while it tended to shift counterclockwise again from 2008 to 2010. This counterclockwise shift indicates that the economic heart of the Pearl River Delta urban agglomeration has been relatively steady and it has remained around the Pearl River Estuary over the past three decades.

3) Urban Expansion Intensity: The urban expansion intensities of the three urban agglomerations were calculated to compare the expansion rates per unit area during 1981–2010. Fig. 10 shows that they experienced rises, falls, and subsequent rises again. The urban expansion intensity of the Pearl River Delta changed the most dramatically and had the highest value compared with the other two urban agglomerations during the first two decades. It reached a peak during 1998–2000, then decreasing markedly, and increasing again in 2003–2005. In the

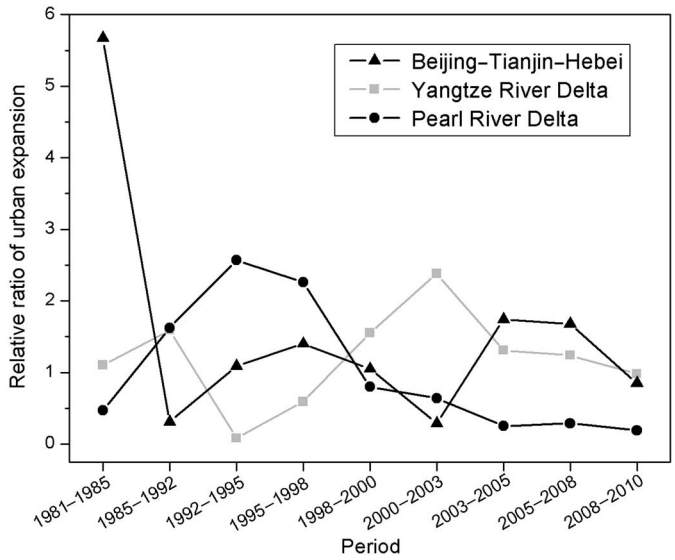

Fig. 11. Relative ratios of urban expansion for the three urban agglomerations. Note that the highest ratios occurred successively in Beijing–Tianjin–Heibei, Pearl River Delta, Yangtze River Delta, and Beijing–Tianjin–Heibei.

Yangtze River Delta, the urban expansion intensity began to exceed that of the Pearl River Delta in 2003–2005, which was followed by a very rapid increase, with the highest level in the final decade. Beijing–Tianjin–Hebei had the lowest urban expansion intensity among the three agglomerations, because it had a point-agglomeration pattern instead of belt-agglomeration pattern, but it also experienced major increases over the past 10 years.

4) Relative Ratio of Urban Expansion: We calculated the ratios of the urban expansion rates of the three urban agglomerations relative to that of China over the past three decades, which fluctuated during different periods, as shown in Fig. 11. Clearly, most of the points were >1, which shows that the expansion rates of the three urban agglomerations were

higher than the average expansion rate in China. However, there were great differences among the regions. The expansion of the Beijing–Tianjin–Hebei urban agglomeration occurred earlier than that of others, which was related to the concentration effects of the capital Beijing. Its relative ratio of urban expansion was much higher than that of the others in the 1980s. The Pearl River Delta urban agglomeration expanded most in the 1990s because of the policy advantages that applied in the Special Economic Zones of Shenzhen and Zhuhai. The Yangtze River Delta and the Beijing–Tianjin–Hebei urban agglomerations predominated successively in the 2000s, which benefited from the rapid development of the Pudong New Area and the Binhai New Area, respectively.

V. Conclusion

Using our proposed method, we detected and analyzed the urban expansion of China during the past 30 years based on DMSP-OLS nighttime light data and NDVI data. During this period, China's urban area experienced a tremendous expansion (11.89 times), as well as the most rapid economic development and urbanization ever known. However, there were high regional variations in the urban expansion. This expansion has profoundly changed the proportion of impervious surface and the local circulation, which will influence the regional climate and thermal environment.

The intercalibration processing based on second-order polynomial regression equations improved the continuity and comparability of the time-series of nighttime light data. According to our visual and quantitative comparisons of the urban boundaries and areas, the proposed local SVM-based region-growing method delivered better performance than the local thresholding method because it required no empirical strategies or manual trial-and-error procedures, while it also outperformed the global SVM-based region-growing method because it implemented the SVM training and region-growing procedures for each economic region. However, more calibration cities could be investigated to make this assessment more convincing.

Among the 30-year urban area products, the accuracies of the urban areas from 1992 to 2010 were better than those from 1981 to 1991 because the NDVI re-labeling method did not work well when the urban areas were converted from other land instead of vegetation areas. Meanwhile, the coarse spatial resolution (5 km) of the NDVI data from 1981 to 1997 produced the relative underestimation of the urban area during this period. The few pseudo-urban pixels in the maps of the Pearl River Delta during the 1980s illustrated these problems. Moreover, the urban areas during the 10 phases illustrated the expansion patterns over 30 years, but the annual products will indicate the key aspects of the expansion procedure more accurately.

The proposed urban expansion rate indicated the national and regional urban growth levels. Moreover, the proposed urban expansion direction, urban expansion intensity, and relative ratio of urban expansion of the typical urban agglomerations indicated the regional variations in China's urban expansion. Clearly, our description of the urban expansion during the three decades based on the proposed method agreed with the economic development situation in China. In future research, more urban agglomerations could be investigated to understand the variations in urban expansion in China more profoundly.

Acknowledgments

The authors wish to thank the NGDC for providing the DMSP-OLS data, the LTDR and SPOT-VGT program for providing the NDVI data, and the UMD and USGS for providing the Landsat images. They also thank Prof. J. Chen and Assoc. Prof. X. Cao of the Beijing Normal University for kindly providing help and suggestions regarding this research. The authors gratefully acknowledge the insightful suggestions, comments, and criticisms from the anonymous reviewers.

References

[1] Q. Zhang and K. C. Seto, "Mapping urbanization dynamics at regional and global scales using multi-temporal DMSP/OLS nighttime light data," *Remote Sens. Environ.*, vol. 115, no. 9, pp. 2320–2329, Sep. 2011.

[2] J. Yin, Z. Yin, H. Zhong, S. Xu, X. Hu, J. Wang, and J. Wu, "Monitoring urban expansion and land use/land cover changes of Shanghai metropolitan area during the transitional economy (1979–2009) in China," *Environ. Monit. Assess.*, vol. 177, no. 1–4, pp. 609–621, Jun. 2011.

[3] F. Fan, Y. Wang, M. Qiu, and Z. Wang, "Evaluating the temporal and spatial urban expansion patterns of Guangzhou from 1979 to 2003 by remote sensing and GIS methods," *Int. J. Geogr. Inf. Sci.*, vol. 23, no. 11, pp. 1371–1388, Nov. 2009.

[4] Y. Ma and R. Xu, "Remote sensing monitoring and driving force analysis of urban expansion in Guangzhou City, China," *Habitat Int.*, vol. 34, no. 2, pp. 228–235, 2010.

[5] C. Xu, M. Liu, C. Zhang, S. An, W. Yu, and J. M. Chen, "The spatiotemporal dynamics of rapid urban growth in the Nanjing metropolitan region of China," *Landscape Ecol.*, vol. 22, no. 6, pp. 925–937, 2007.

[6] J. Xiao, Y. Shen, J. Ge, R. Tateishi, C. Tang, Y. Liang, and Z. Huang, "Evaluating urban expansion and land use change in Shijiazhuang, China, by using GIS and remote sensing," *Landscape Urban Plan.*, vol. 75, no. 1–2, pp. 69–80, Feb. 2006.

[7] M. Tan, X. Lia, H. Xie, and C. Lu, "Urban land expansion and arable land loss in China–a case study of Beijing–Tianjin–Hebei region," *Land Use Policy*, vol. 22, no. 3, pp. 187–196, Jul. 2005.

[8] C. He, J. Li, J. Chen, P. Shi, J. Chen, Y. Pan, J. Li, L. Zhuo, and T. Ichinose, "The urbanization process of Bohai Rim in the 1990s by using DMSP/OLS data," *J. Geogr. Sci.*, vol. 16, no. 2, pp. 174–182, May 2006.

[9] G. Tian, J. Jiang, Z. Yang, and Y. Zhang, "The urban growth, size distribution and spatio-temporal dynamic pattern of the Yangtze River Delta megalopolitan region, China," *Ecol. Model.*, vol. 222, no. 3, pp. 865–878, Feb. 2011.

[10] X. Li and A. G. O. Yeh, "Principal component analysis of stacked multi-temporal images for the monitoring of rapid urban expansion in the Pearl River Delta," *Int. J. Remote Sens.*, vol. 19, no. 8, pp. 1501–1518, 1998.

[11] A. G. O. Yeh and X. Li, "Economic development and agricultural land loss in the Pearl River Delta, China," *Habitat Int.*, vol. 23, no. 3, pp. 373–390, Sep. 1999.

[12] Q. Weng, "A remote sensing-GIS evaluation of urban expansion and its impact on surface temperature in the Zhujiang Delta, China," *Int. J. Remote Sens.*, vol. 22, no. 10, pp. 1999–2014, 2001.

[13] S. Chen, S. Zeng, and C. Xie, "Remote sensing and GIS for urban growth analysis in China," *Photogramm. Eng. Remote Sens.*, vol. 66, no. 5, pp. 593–598, May 2000.

[14] C. Y. Ji, Q. Liu, D. Sun, S. Wang, P. Lin, and X. Li, "Monitoring urban expansion with remote sensing in China," *Int. J. Remote Sens.*, vol. 22, no. 8, pp. 1441–1455, 2001.

[15] G. Tian, J. Liu, Y. Xie, Z. Yang, D. Zhuang, and Z. Niu, "Analysis of spatio-temporal dynamic pattern and driving forces of urban land in China in 1990s using TM images and GIS," *Cities*, vol. 22, no. 6, pp. 400–410, Dec. 2005.

[16] X. Deng, J. Huang, S. Rozelle, and E. Uchida, "Growth, population and industrialization, and urban land expansion of China," *J. Urban Econ.*, vol. 63, no. 1, pp. 96–115, Jan. 2008.

[17] X. Deng, J. Huang, S. Rozelle, and E. Uchida, "Economic growth and the expansion of urban land in China," *Urban Stud.*, vol. 47, no. 4, pp. 813–843, Apr. 2010.

[18] L. Wang, C. Li, Q. Ying, X. Cheng, X. Wang, X. Li, L. Hu, L. Liang, L. Yu, H. Huang, and P. Gong, "China's urban expansion from 1990 to 2010 determined with satellite remote sensing," *Chin. Sci. Bull.*, vol. 57, no. 22, pp. 2802–2812, Aug. 2012.
[19] N. Levin and Y. Duke, "High spatial resolution night-time light images for demographic and socio-economic studies," *Remote Sens. Environ.*, vol. 119, pp. 1–10, Apr. 2012.
[20] T. Ma, C. Zhou, T. Pei, S. Haynie, and J. Fan, "Quantitative estimation of urbanization dynamics using time series of DMSP/OLS nighttime light data: A comparative case study from China's cities," *Remote Sens. Environ.*, vol. 124, pp. 99–107, Sep. 2012.
[21] C. D. Elvidge, K. E. Baugh, J. B. Dietz, T. Bland, P. C. Sutton, and H. W. Kroehl, "Radiance calibration of DMSP-OLS low light imaging data of human settlements," *Remote Sens. Environ.*, vol. 68, no. 1, pp. 77–88, Apr. 1999.
[22] C. D. Elvidge, M. L. Imhoff, K. E. Baugh, V. R. Hobson, I. Nelson, J. Safran, J. B. Dietz, and B. T. Tuttle, "Nighttime lights of the world: 1994–1995," *ISPRS J. Photogramm.*, vol. 56, no. 2, pp. 81–99, Dec. 2001.
[23] C. P. Lo, "Urban indicators of China from DN-calibrated digital DMSP-OLS nighttime images," *Ann. Assoc. Amer. Geogr.*, vol. 92, no. 2, pp. 225–240, 2002.
[24] X. Cao, J. Chen, H. Imura, and O. Higashi, "A SVM-based method to extract urban areas from DMSP-OLS and SPOT VGT data," *Remote Sens. Environ.*, vol. 113, no. 10, pp. 2205–2209, Oct. 2009.
[25] Z. Liu, C. He, Q. Zhang, Q. Huang, and Y. Yang, "Extracting the dynamics of urban expansion in China using DMSP-OLS nighttime light data from 1992 to 2008," *Landscape Urban Plan.*, vol. 106, no. 1, pp. 62–72, May 2012.
[26] B. Pandey, P. K. Joshi, and K. C. Seto, "Monitoring urbanization dynamics in India using DMSP/OLS night time lights and SPOT-VGT data," *Int. J. Appl. Earth Obs.*, vol. 23, pp. 49–61, Aug. 2013.
[27] C. D. Elvidge, K. E. Baugh, E. A. Kihn, H. W. Kroehl, E. R. Davis, and C. W. Davis, "Relation between satellite observed visible-near infrared emissions, population, economic activity and electric power consumption," *Int. J. Remote Sens.*, vol. 18, no. 6, pp. 1373–1379, 1997.
[28] C. P. Lo, "Modeling the population of China using DMSP Operational Linescan System nighttime data," *Photogramm. Eng. Remote Sens.*, vol. 67, no. 9, pp. 1037–1047, Sep. 2001.
[29] P. C. Sutton, "A scale-adjusted measure of 'urban sprawl' using nighttime satellite imagery," *Remote Sens. Environ.*, vol. 86, no. 3, pp. 353–369, Aug. 2003.
[30] S. Amaral, A. M. V. Monteiro, G. Camara, and J. A. Quintanilha, "DMSP/OLS night-time light imagery for urban population estimates in the Brazilian Amazon," *Int. J. Remote Sens.*, vol. 27, no. 5, pp. 855–870, Mar. 2006.
[31] L. Zhuo, T. Ichinose, J. Zheng, J. Chen, P. Shi, and X. Li, "Modelling the population density of China at the pixel level based on DMSP/OLS non-radiance-calibrated night-time light images," *Int. J. Remote Sens.*, vol. 30, no. 4, pp. 1003–1018, Feb. 2009.
[32] W. Wang, H. Cheng, and L. Zhang, "Poverty assessment using DMSP/OLS night-time light satellite imagery at a provincial scale in China," *Adv. Space Res.*, vol. 49, no. 8, pp. 1253–1264, Apr. 2012.
[33] C. D. Elvidge, D. Ziskin, K. E. Baugh, B. T. Tuttle, T. Ghosh, D. W. Pack, E. H. Erwin, and M. Zhizhin, "A fifteen-year record of global natural gas flaring derived from satellite data," *Energies*, vol. 2, no. 3, pp. 595–622, Aug. 2009.
[34] X. Li, F. Chen, and X. Chen, "Satellite-observed nighttime light variation as evidence for global armed conflicts," *IEEE J-STARS*, vol. 6, no. 5, pp. 2302–2315, Oct. 2013.
[35] C. Small, F. Pozzi, and C. D. Elvidge, "Spatial analysis of global urban extent from DMSP-OLS night lights," *Remote Sens. Environ.*, vol. 96, no. 3–4, pp. 277–291, Jun. 2005.
[36] M. L. Imhoff, W. T. Lawrence, D. C. Stutzer, and C. D. Elvidge, "A technique for using composite DMSP/OLS City Lights satellite data to accurately map urban areas," *Remote Sens. Environ.*, vol. 61, no. 3, pp. 361–370, Sep. 1997.
[37] C. D. Elvidge, K. E. Baugh, E. A. Kihn, H. W. Kroehl, and E. R. Davis, "Mapping city lights with nighttime data from the DMSP Operational Linescan System," *Photogramm. Eng. Remote Sens.*, vol. 63, no. 6, pp. 727–734, Jun. 1997.
[38] C. Milesi, C. D. Elvidge, R. R. Nemani, and S. W. Running, "Assessing the impact of urban land development on net primary productivity in the southeastern United States," *Remote Sens. Environ.*, vol. 86, no. 3, pp. 401–410, Aug. 2003.
[39] M. L. Imhoff, W. T. Lawrence, C. D. Elvidge, T. Paul, E. Levine, M. V. Prevalsky, and V. Brown, "Using nighttime DMSP/OLS images of city lights to estimate the impact of urban land use on soil resources in the U.S.," *Remote Sens. Environ.*, vol. 59, no. 1, pp. 105–117, Jan. 1997.
[40] C. He, P. Shi, J. Li, J. Chen, Y. Pan, J. Li, L. Zhuo, and T. Ichinose, "Restoring urbanization process in China in the 1990s by using non-radiance calibrated DMSP/OLS nighttime light imagery and statistical data," *Chin. Sci. Bull.*, vol. 51, no. 13, pp. 1614–1620, Jul. 2006.
[41] M. Henderson, E. T. Yeh, P. Gong, C. Elvidge, and K. Baugh, "Validation of urban boundaries derived from global night-time satellite imagery," *Int. J. Remote Sens.*, vol. 24, no. 3, pp. 595–609, 2003.
[42] D. Lu, H. Tian, G. Zhou, and H. Ge, "Regional mapping of human settlements in southeastern China with multisensor remotely sensed data," *Remote Sens. Environ.*, vol. 112, no. 9, pp. 3668–3679, Sep. 2008.
[43] X. Hu, "On the typology and organization of economic regions in China," *Acta Geogr. Sin.*, vol. 48, no. 3, pp. 193–203, May 1993.
[44] G. M. Foody and A. Mathur, "The use of small training sets containing mixed pixels for accurate hard image classification: Training on mixed spectral responses for classification by a SVM," *Remote Sens. Environ.*, vol. 103, no. 2, pp. 179–189, Jul. 2006.
[45] C. Fang, J. Song, Q. Zhang, and M. Li, "The formation, development and spatial heterogeneity patterns for the structures system of urban agglomerations in China," *Acta Geogr. Sin.*, vol. 60, no. 5, pp. 827–840, Sep. 2005.
[46] J. Liu, H. Tian, M. Liu, D. Zhuang, J. M. Melillo, and Z. Zhang, "China's changing landscape during the 1990s: Large-scale land transformations estimated with satellite data," *Geophys. Res. Lett.*, vol. 32, no. 2, pp. 1–5, Feb. 2005.

Pengfeng Xiao (M'13) was born in Hunan, China, in 1979. He received the B.S. degree in land resource management from Hunan Normal University, Changsha, China, in 2002, and the Ph.D. degree in cartography and geographical information system from Nanjing University, Nanjing, China, in 2007.

From 2007 to 2009, he was a Lecturer with the Department of Geographic Information Science, Nanjing University. Since 2009, he has been an Associate Professor with the Department of Geographic Information Science, Nanjing University. He is the author of two books and more than 40 articles. He is the holder of one patent and two software programs. His research interests include remote sensing image processing, land use and land cover change, and remote sensing of snow cover.

Dr. Xiao was a recipient of the Geographical Society of China (GSC) Prize for Best Paper by Young Author in 2006, the Chinese Professional in Geographic Information Systems (CPGIS) Best Student Paper Award (first place) in 2007, and the International Society for Photogrammetry and Remote Sensing (ISPRS) Prize for Best Paper by Young Author in 2008.

Xiaohui Wang was born in Anhui, China, in 1989. She received the B.E. degree in surveying and mapping engineering from Anhui University of Architecture, Hefei, China, in 2010, and the M.S. degree in cartography and geographical information system from Nanjing University, Nanjing, China, in 2013.

Currently, she is working with Hefei National High-Tech Industrial Development Zone, Hefei, China. She is the author of two articles. Her research interests include land use and land cover change, and remote sensing image processing.

Xuezhi Feng was born in Gansu, China in 1953. He received the B.S. degree in cartography from Nanjing University, Nanjing, China, in 1979.

From 1980 to 1981, he was a Lecturer with the Department of Geography, Nanjing University. He was then employed by the Lanzhou Institute of Glaciology and Cryopedology, Chinese Academy of Sciences, Lanzhou, China, as an Assistant Professor from 1981 to 1990, as an Associate Professor from 1990 to 1994, and as a Professor from 1994 to 1997. Since 1997, he has been a Professor with the Department of Geographic Information Science, Nanjing University. He is the author of

four books and more than 200 articles. His research interests include remote sensing of snow cover, snowmelt water resource, and remote sensing image processing.

Prof. Feng is the Executive Council Member of the China Association of Remote Sensing Application (CARSA) and the Honorary Council Member of the Associate on Environment Remote Sensing of China (AERSC).

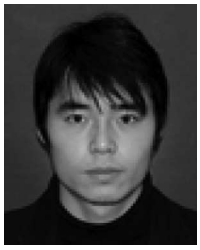

Xueliang Zhang was born in Hunan, China, in 1987. He received the B.S. degree in geographical information system from Nanjing University, Nanjing, China, in 2010. Currently, he is working toward the Ph.D. degree in cartography and geographical information system at Nanjing University.

He is the author of four articles published in international journals. His research interests include remote sensing image processing and high-resolution remote sensing image segmentation.

Mr. Zhang was a recipient of the Best Student Paper Award (first place) in the Second International Workshop on Earth Observation and Remote Sensing Applications, Shanghai, China, in 2012.

Yongke Yang was born in Henan, China, in 1987. He received the B.S. degree in geographical information system from Xuchang University, Henan, China, in 2011. Currently, he is working toward the M.S. degree in cartography and geographical information system at Nanjing University, Nanjing, China.

He is the author of one article. His research interests include land use and land cover change, and remote sensing image processing.